nature energy

ARTICLES

PUBLISHED: 26 SEPTEMBER 2016 | ARTICLE NUMBER: 16151 | DOI: 10.1038/NENERGY.2016.151

Photocatalytic hydrogen production using twinned nanocrystals and an unanchored NiS_x co-catalyst

Maochang Liu*, Yubin Chen, Jinzhan Su, Jinwen Shi, Xixi Wang and Liejin Guo*

Facilitating charge separation as well as surface redox reactions is considered to be central to improving semiconductor-catalysed solar hydrogen generation. To that end, photocatalysts comprising intimately interfaced photo absorbers and co-catalysts have gained much attention. Here, we combine an efficient $Cd_{0.5}Zn_{0.5}S$ (CZS) nanotwinned photocatalyst with a NiS_x co-catalyst for photogeneration of hydrogen. We find that an internal quantum efficiency approaching 100% at 425 nm can be achieved for photocatalytic H_2 production from water with Na_2S/Na_2SO_3 as hole scavengers. Our results indicate that the NiS_x co-catalyst is not anchored on the surface of the host CZS nanotwins and instead exists in the reaction solution as freestanding subnanometre clusters. We propose that charge transfer is accomplished via collisions between the CZS and NiS_x clusters, which aids charge separation and inhibits back reaction, leading to high water reduction rates in the suspension.

Photocatalytic hydrogen production from water using semiconductor photocatalysts has been considered 'green' for solar energy conversion. The pioneering work can be traced back to 1972 when Fujishima and Honda reported the photoelectrochemical hydrogen production catalysed by titanium dioxide[1]. However, further commercial development of the technology, as well as large-scale manufacture of photocatalysts, is still restricted by their low activity and high cost[2].

The activity of photocatalytic reaction has long relied on facilitating charge separation and surface redox reaction[2–5]. The last decades have witnessed the success of fabricating heterojunction photocatalysts by coupling two or more materials at the nanoscale to this end. Examples include sulfides[6,7], oxides[8,9], nitrides[10] and their combinations[11–16]. However, most of the reported junctions were based on a further addition of noble metal co-catalysts. Development of noble metal-free photocatalysts that can be readily used for low-cost and pilot system design is thus significantly favoured, but still challenging to date. In principle, the electron capture by a co-catalyst nanoparticle provides the most powerful means to manipulate the reduction rate of H^+ in the reaction solution[9,13,17–19]. Interest in co-catalyst nanoparticles therefore has been growing steadily during the past decades. Thanks to the efforts of many groups, some non-precious metal-containing co-catalysts, for example, Ni[6,20–24], Co[19,25], Cu[26,27] and their oxidative species have been developed. By forming an intimate heterojunction with the primary photocatalyst, these co-catalysts were found with potential capability for accelerating hydrogen production. Unfortunately, attempts to achieve high activity over noble metal-free heterojunctions have still met limited success.

Herein, we present a photocatalytic system in which the NiS_x co-catalyst is proposed to exist as freestanding subnanometre clusters, rather than being intimately attached to the $Cd_{0.5}Zn_{0.5}S$ (CZS) twinned nanorod photocatalyst. These clusters are suggested to provide active hydrogen production sites after accepting photogenerated electrons by collision with the CZS photocatalyst. Due to the isolated state of the co-catalyst, back reaction is efficiently inhibited. Such a synergy created by the primary photocatalyst and co-catalyst gave rise to nearly 100% internal quantum efficiency at 425 nm for hydrogen production from aqueous solution using Na_2S/Na_2SO_3 as hole scavengers. Moreover, the proposed mechanism was also extended to and validated by other nanoparticle systems with, for example, CdS or CdSe as primary photocatalysts, or Pt as a co-catalyst. This work thus suggests an avenue for developing high-efficiency and noble metal-free photocatalytic systems.

Photocatalytic behaviour

A CZS nanorod photocatalyst with a twin structure was prepared according to our previous reported methods[28]. Visible-light-driven hydrogen production ($\lambda \geq 430$ nm) was initiated by injecting a certain amount of Ni^{2+} ions into a suspension containing CZS, Na_2S and Na_2SO_3. Figure 1a shows the average rates of H_2 evolution during the first 5-h reaction over the CZS photocatalysts by adding different amounts of Ni^{2+} (denoted as Twin-Ni-I). Clearly, a volcano-like distribution of the activities for hydrogen production was obtained, with the highest rate, that is, 4.46 mmol h^{-1} at 0.03 wt% Ni^{2+}. This efficiency is about 1.7 times that of the pure CZS that has been demonstrated already with excellent charge separation property by a twin-induced ordered homojunction[28,29]. We then measured the apparent quantum efficiencies on this photocatalyst at different light wavelengths by using various band-pass filters in the same reaction solution (see Supplementary Table 1 for details). The trend in apparent quantum efficiency closely followed that of the absorbance measured by ultraviolet–visible spectroscopy (Fig. 1b), revealing bandgap-transition-dependent hydrogen evolution behaviour[30,31]. Notably, a high apparent quantum efficiency of about 94% was obtained at 425 nm (see Supplementary Fig. 1a for the optical property of the filter). Considering the transmittance of the Pyrex cell, that is, around 95% (Supplementary Fig. 1b), the internal quantum efficiency is estimated to be approaching 100%. In other words, one photon excites one electron/hole pair that can completely convert a proton into a hydrogen atom. Bubbles evolved from a fixed film photocatalyst allow us to visualize photon-to-hydrogen conversion. To this end, a thin layer of CZS twinned nanorods was attached to fluorine-doped tin oxide (FTO) glass through an

International Research Center for Renewable Energy, State Key Laboratory of Multiphase Flow in Power Engineering, Xi'an Jiaotong University, Xi'an, Shaanxi 710049, China. *e-mail: maochangliu@mail.xjtu.edu.cn; lj-guo@mail.xjtu.edu.cn

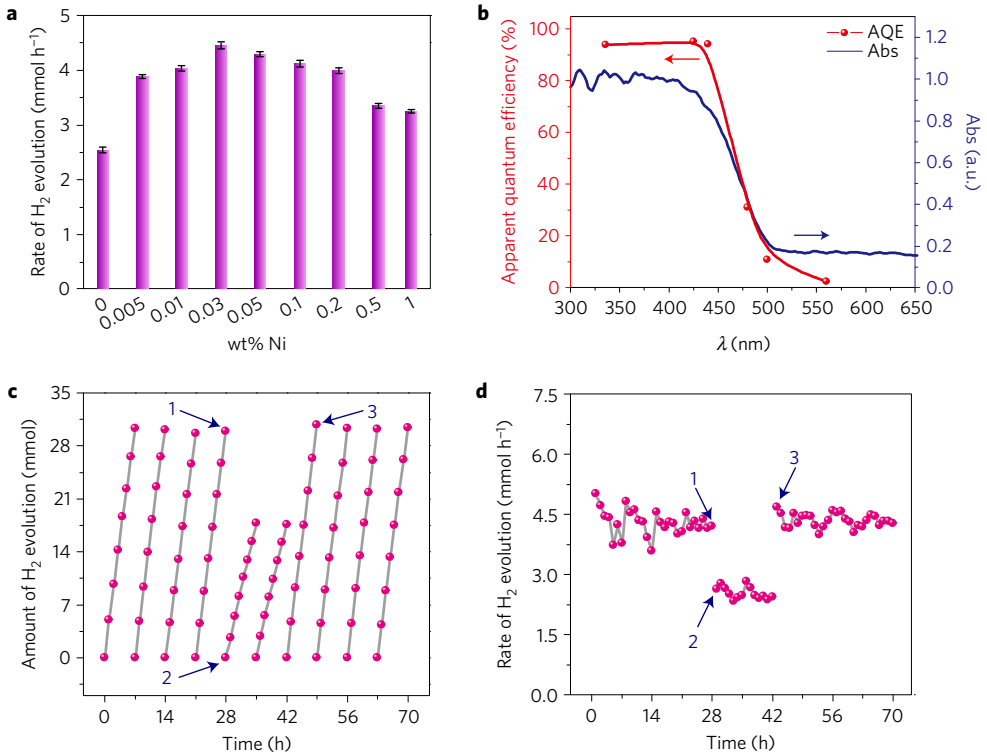

Figure 1 | Photocatalytic performance of CZS-based photocatalysts. a, Initial rate of hydrogen evolution over CZS twinned photocatalysts with different Ni content calculated from the first 5 h of the test. Error bars in **a** are standard error values of three tests (n = 3). **b**, Ultraviolet–visible absorbance spectrum and apparent quantum efficiency for Twin-Ni-I with 0.03 wt% Ni. **c**, Time course of hydrogen evolution on the Twin-Ni-I photocatalyst when using a Ni^{2+} concentration of 0.03 wt%. The reaction was stopped and flushed with N_2 every 7 h due to the large amount of H_2 gas generated. **d**, Corresponding hydrogen evolution rate at each hour during the 70-h test. The points marked in **c** and **d** indicate (1) the actions of centrifugation of the original reaction, (2) re-dispersion of the obtained photocatalyst into a fresh Na_2S-Na_2SO_3 solution without adding additional Ni^{2+}, and (3) injection of additional 0.03 wt% Ni^{2+}, respectively.

electrophoretic-deposition process. After the fixed photocatalyst was placed in the same reaction solution (Na_2S/Na_2SO_3), many bubbles were observed on the film (Supplementary Video 1). When 0.03 wt% Ni^{2+} was injected into the suspension, the reaction was significantly accelerated. As shown in Supplementary Video 2, a much larger amount of H_2 bubbles evolved from the film. We also investigated the pH-dependent photocatalytic activity by adding different amounts of concentrated sulfuric acid (H_2SO_4, 98%) into the reaction mixture. Similar to the previous reports[16,32], a higher pH value of the reaction solution led to enhanced photocatalytic activity of CZS (Supplementary Fig. 2). However, our system still maintained an apparent quantum efficiency of ~64% (425 nm) even when the pH was reduced to 12.87.

Moreover, the Twin-Ni-I photocatalyst also exhibited a relatively high stability in this reaction solution. Our time-course photocatalytic test over the 0.03 wt% Ni combined twinned nanorods indicated no obvious decrease for hydrogen generation for the initial 28 h (Fig. 1c,d, 0–28 h). Afterwards, the photocatalyst was separated from the reaction solution by centrifugation (at a rate of 4,000 r.p.m. for 10 min). We continued the same test by re-dispersing the photocatalyst into a fresh Na_2S-Na_2SO_3 solution. It showed an identical photocatalytic behaviour compared to pure CZS twinned nanorods. The hydrogen evolution rate unexpectedly dropped to 2.64 mmol h^{-1}, and the activity was well maintained for another 14 h (Fig. 1c,d, 28–42 h). Interestingly and more importantly, addition of another 0.03 wt% Ni^{2+} into the same reaction solution recovered the activity (Fig. 1c,d, 42–70 h). These results imply that Ni species contribute to the improved photocatalytic activity, yet in a different manner from a traditional intimate heterojunction.

X-ray photoelectron spectroscopy and microscopy study

We next sought to determine whether Ni species were anchored on the surface of CZS nanorods during the reaction. To this end, 0.03 wt%, 1 wt% and 3 wt% Ni-containing Twin-Ni-I photocatalysts were examined by X-ray photoelectron spectroscopy (XPS, see Supplementary Fig. 3). We also prepared a mixture of CZS and the Ni-based co-catalyst by sequential addition of Ni^{2+} and the twinned nanorods (in this case, formation of Ni-based co-catalyst would not be impacted by CZS) into the Na_2S/Na_2SO_3 solution as a reference (denoted as Twin-Ni-I'). However, no notable XPS peaks corresponding to the binding energies of Ni 2p were detected in these four samples[33]. It indicated that no Ni-based co-catalyst was adsorbed on the surface of these twinned nanorod photocatalysts. We then investigated the microstructures of Twin-Ni-I by using a transmission electron microscope (TEM) and a high-resolution scanning TEM (HRSTEM). As shown in Supplementary Fig. 4a and the inset, despite the addition of even 3 wt% Ni, the photocatalyst was characterized only by monodispersed nanorods, showing no trace of co-catalyst nanoparticles. A careful examination by HRSTEM and the corresponding fast Fourier transform measurements (Supplementary Fig. 4b,c) with ordered changes in atom arrangement and diffraction spots clearly demonstrated the densely existing twin boundaries[28,29]. Note that even though the sample experienced a 70-h photocatalytic reaction, Ni species remained undetectable by TEM and XPS examination (Supplementary Fig. 5). An XPS survey spectrum and high-resolution spectra of the other elements over 0.03% Ni-containing Twin-Ni-I were also provided (corrected by setting the C 1s line to 284.50 eV), which certified the typical chemical states of Cd^{2+}, Zn^{2+}, and S^{2-}, respectively (Supplementary Fig. 6)[33]. Both XPS and TEM

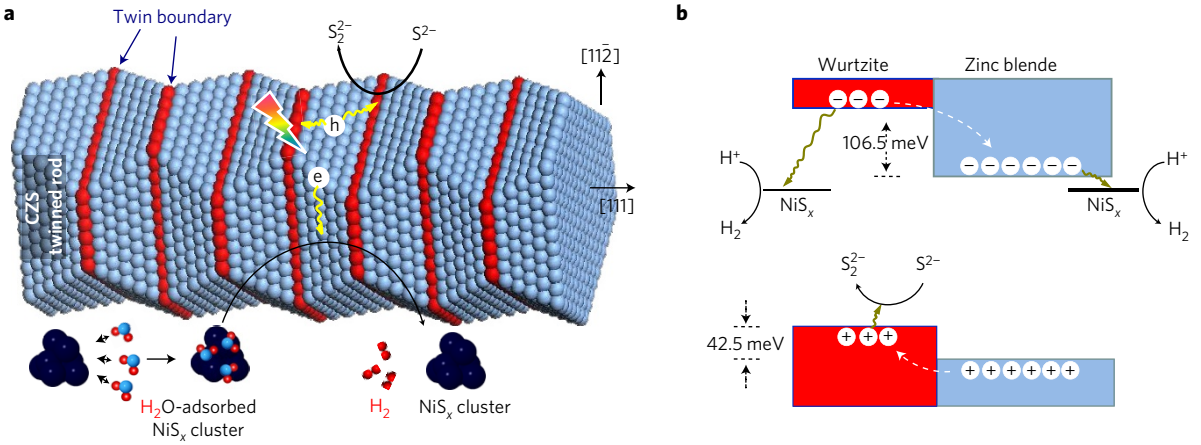

Figure 2 | Proposed mechanism involved in the Twin-Ni-I-based photocatalytic process. a, Schematic illustration of the suggested mechanism whereby NiS_x and CZS nanorods undergo collisions to transfer photogenerated electrons. The NiS_x clusters are proposed to serve as a reaction centre for H_2 evolution. **b**, Band alignment around a twin boundary in CZS and the photocatalytic process involving charge separation and surface redox reaction. In both panels, red indicates wurtzite and blue indicates zinc blende crystal phases.

analyses again suggested that the co-catalyst was not adsorbed on the surface of the CZS twinned rods.

Proposed photocatalytic mechanism

The Twin-Ni-I' photocatalyst (0.03 wt% Ni) also showed improved photocatalytic activity with an initial H_2 evolution rate of 4.26 mmol h^{-1}, close to that of the Twin-Ni-I photocatalyst (Supplementary Fig. 7). More importantly, the similar photocatalytic behaviour after separating/re-dispersing of the CZS photocatalyst indicates that Ni in Twin-Ni-I' and Twin-Ni-I should occupy an identical chemical state and thus play the same role for enhanced photoactivity. Given the concentrated S^{2-} ions in the reaction solution, it is believed that the co-catalyst should be primarily composed of NiS_x. This multi-valence-state feature of Ni was also supported by the electron paramagnetic resonance spectra with clearly observed electron spin signal derived from the unpaired electrons (Supplementary Fig. 8). In addition, the size of NiS_x should be very small as it could not be separated from the reaction solution with the conventional low-speed centrifugation. It is also worth pointing out that our experiment by introducing Ni^{2+} into a similar reaction without adding CZS showed no substantial activity for H_2 evolution. It suggests that NiS_x itself could not be visible-light activated or act as a photocatalyst alone. However, when at an intermediate state excited by accepting electrons from CZS, it will show the power for H_2 production. In principle, Ni has been found with a relatively small heat for hydrogen adsorption (about 109 ~ 134 kJ mol^{-1} for Ni and 109 kJ mol^{-1} for Pt)[34]. In addition, according to the relationship between the exchange current for H_2 evolution and the M–H (M represents a transitional metal) bond strength, Ni, among all the non-precious metals, shows the lowest activation energy, which is even comparable to Pt for H_2 evolution[19,35]. These notions explain the possible role of Ni or its oxidized counterpart during proton reduction compared with Pt: they will contribute to the enhancement of the mass transfer process by facilitating the adsorption–reduction–desorption process of hydrogen.

A photocatalytic system with soluble CdSe nanocrystals as the light absorber and soluble Ni^{2+}-dihydrolipoic acid as the proton reduction catalyst was recently presented[20]. It was demonstrated that this homogeneous system, without having nickel catalyst deposited on the surface of CdSe nanocrystal, showed a high quantum efficiency of more than 36% for hydrogen production. In our case, we may anticipate NiS_x as an isolated colloidal co-catalyst. Moreover, due to the surrounding alkaline environment, free H^+ ions can hardly exist. The reaction is supposed to proceed through the Volmer–Heyrovsky or Volmer–Tafel pathways, in which H_2 production will be in the form of direct reduction of H_2O molecules, instead of dissociated H^+ ions, on the surface of the catalyst[36,37]. The NiS_x-based enhanced photocatalytic process thus can be hypothesized as via a collision-contact mechanism as shown Fig. 2a. For the first step, NiS_x may readily form a Ni–H bond with the adsorbed H_2O at its surface. At the second step, these H_2O-bonded NiS_x clusters collide with CZS nanorods, by which, a portion of photogenerated electrons were transferred to NiS_x. The activated clusters then serve as a reaction centre for H_2O reduction and H_2 evolution. Figure 2b shows a schematic illustration of the corresponding band alignment and the related charge transportation process. Specifically, photoexcited electrons from either the wurtzite (WZ) or zinc blende (ZB) segment can be transferred to NiS_x to induce water reduction. Because of the existent WZ–ZB homojunction originated from twin boundaries[28], photoexcited holes, on the contrary, will be repelled or localized to the WZ region (around twin boundary) regardless of its generation site. Notably, given the already possessed activity of CZS twinned photocatalyst for H^+ reduction, our proposed mechanism will not exclude the possibility of the reduction on the surface of nanotwins. Only after collision, the water reduction occurring on the NiS_x co-catalyst becomes possible. Obviously, one important advantage of such a manner of interaction between substrate photocatalyst and co-catalyst is that it can actively inhibit back reaction and therefore gain a very high hydrogen generation rate in the suspension.

Validation of the mechanism

To eliminate the impact of the host photocatalyst and elucidate the mechanism in a more clear way, we turned back to the similar process using CZS twinned film instead of twinned powder as the photocatalyst, as schematically illustrated in Supplementary Fig. 9. Specifically, by fixing the primary photocatalyst on the FTO glass, the process involving collision can be tracked via simply quantifying the content of Ni^{2+} in the solution. We firstly evaluated the hydrogen production property of the film photocatalyst with or without addition of Ni^{2+} (the same amount as that used in the 0.03 wt% Ni-containing particle-suspension system, that is, 0.17 μg ml^{-1}). As shown in Fig. 3a, introduction of such a trace amount of Ni^{2+} could, as anticipated, approximately double the photocatalytic activity. We then measured the content of Ni in the reaction by analysing aliquots of the reaction solution from the photolysis every 20 min using an inductively coupled plasma mass spectrometer (ICP-MS, Fig. 3b). Clearly, the result suggested a steady concentration of Ni

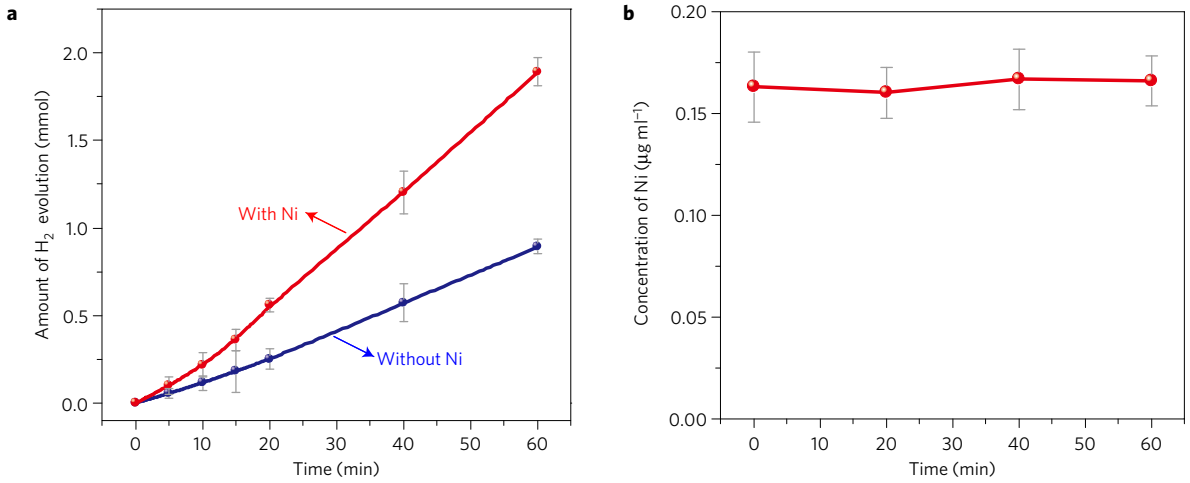

Figure 3 | Photocatalytic performance of CZS films. a, Hydrogen evolution over the CZS film photocatalysts with or without the introduction of 0.03 wt% Ni^{2+}. **b**, Concentration of Ni in the reaction solution during the photocatalytic reaction determined by ICP-MS. Error bars in **a** and **b** are standard error values of three tests (n = 3).

in the reaction solution without showing any loss of mass, and thus provided evidence of the absence of any physical adsorption of Ni species on the surface of CZS photocatalyst. To gain a better understanding toward the explicit state of NiS_x, the reaction solution after 1-h reaction was further characterized by the dynamic light scattering (DLS) method. As shown in Fig. 4a (as generated from Supplementary Fig. 10), the size of NiS_x was determined to be as small as 0.62 nm. It is also interestingly found that the size gradually increased as the concentration of Ni^{2+} increased from 0.03 wt% to 1 wt% and eventually reached 5.51 nm when 3 wt% Ni^{2+} was introduced. The result is in good accordance with the TEM observations (Supplementary Fig. 11), in which the samples were obtained by ultracentrifugation of the suspension from the film system (50,000 r.p.m., 30 min). In particular, the sample shown in Supplementary Fig. 11a (with 1 wt% Ni^{2+}) was further investigated by a collective use of XPS and high-resolution TEM (Fig. 4b–d). The higher binding energies of Ni than that in NiS, an interplanar spacing of 0.31 nm, and the defective lattice arrangement directly demonstrated the formation of NiS_x.

We then applied ultracentrifugation to separate Twin-Ni-I photocatalyst from the reaction mixture containing suspended CZS and NiS_x (containing 3 wt% Ni). The resultant product was washed with deionized water and sampled for TEM observation. As shown in Supplementary Fig. 12, many isolated NiS_x nanoparticles locate nearby the CZS nanotwins, suggesting only loose contact between the two materials. A reaction mixture containing suspended CZS and NiS_x was also analysed by DLS. Since the concentration of Ni in the original reaction solution is very low compared with CZS nanotwins, the sampling solution for the DLS measurement is a little different. We firstly prepared NiS_x by adding 3 wt% Ni^{2+} into the Na_2S-Na_2SO_3 solution. CZS nanotwins with a mole ratio of CZS/Ni = 1:1 were then added to the above solution. After photoreaction for 1 h, the suspension was characterized by DLS. As shown in Supplementary Fig. 13, two distinguished peaks at about 5.85 and 307.6 nm belonging to NiS_x and CZS nanotwins, respectively, can be clearly viewed, in accordance with the TEM observation. These results indicate that we may selectively control the nanostructures of a given co-catalyst without modifying the primary photocatalyst. For example, when we tried to produce close-contacted CZS and NiS_x photocatalyst (0.03 wt% Ni-containing, Twin-Ni-C), larger NiS_x nanoparticles attached on the surface of CZS nanotwins were obtained (Supplementary Fig. 14a). This size increment resulted in a reduced enhancement of the activity with an apparent quantum efficiency of about 74% at 425 nm (Supplementary Fig. 14b). In addition, it was found that the reactivity of the heterojunction photocatalyst is not influenced by the operation of centrifugation and re-dispersion, suggesting different catalytic mechanisms may be at play in the Twin-Ni-C and Twin-Ni-I photocatalysts.

While the above result exemplified the subnanometre behaviour of NiS_x, it did not reveal why these clusters could stably exist. To this end, zeta potential measurement, one of the most effective method to validate the quality of the cluster stability, was carried out[38]. The zeta potentials of sole NiS_x (obtained from the film system shown in Supplementary Fig. 9), CZS twin, and CZS Twin-Ni-I (obtained from suspension system) are summarized in Supplementary Table 2. Clearly, particles in the four sets of suspensions were all negatively charged. In spite of the relatively low absolute value, negative potentials of both CZS twin and NiS_x could contribute to the isolating state of NiS_x even after their collision with each other. On the other hand, just owing to the not too high absolute zeta potential, collision between H_2O-adsorbed NiS_x and CZS nanotwins can frequently occur through Brownian motion. It is worth noting that the current system has differences compared with previous studies of the chalcogenide photocatalysts[16,32,39]. In these studies, high efficiencies for solar H_2 production were achieved over close-contact heterojunctions. Our work is therefore considered to provide a different pathway for improving the photocatalytic activity.

Extension to other photocatalytic systems

To investigate the generality of our proposed mechanism, we also conducted similar photocatalytic measurements over CdS and CdSe photocatalysts. Both of these two photocatalysts were hydrothermally prepared and characterized by nanosized crystals (Supplementary Fig. 15a,b). Although CdS and CdSe showed poor performance for H_2 production, that is, ~0.014 and ~0.017 mmol h^{-1}, respectively, their activities have been substantially improved by adding 0.03 wt% Ni^{2+} into the reaction solution (Supplementary Fig. 15c,d). The apparent quantum efficiencies (425 nm) were measured to be 54% and 32%, for the NiS_x-containing CdS and CdSe photocatalysts, respectively. Both efficiencies were improved by more than 100 times compared with the naked primary photocatalysts. More importantly, they were found with the same photocatalytic behaviour as CZS photocatalyst. As shown in Supplementary Fig. 15c,d, the primary photocatalyst, separated by centrifugation (at a rate of 4,000 r.p.m. for 10 min) and re-dispersed into the same reaction solution, showed low H_2 evolution again. The enhanced activity can be recovered as soon as 0.03 wt% Ni^{2+} is introduced again.

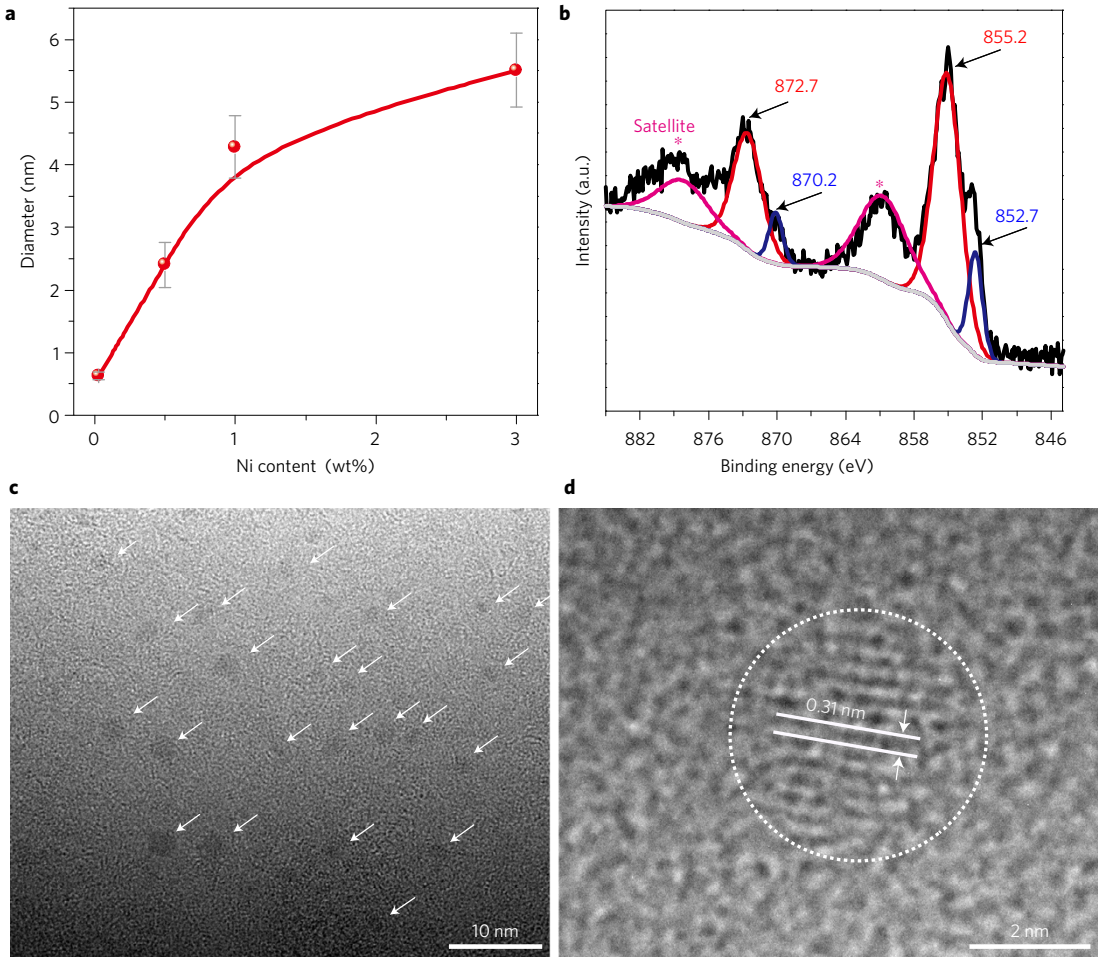

Figure 4 | Characterization of the freestanding NiS_x particles. a, Size distribution of the NiS_x with different concentrations of Ni after 1-h reaction in the film system obtained from the DLS measurements and fitted via B-spline approximation. Error bars in **a** are standard error values obtained based on three time measurements (n = 3). **b**, XPS spectrum of the NiS_x particles (Ni 2p scan) obtained from the film system with a mass fraction of 1 wt% of Ni after 1-h reaction. The spectrum was further fitted by taking the Shirley background and according to the Gaussian–Lorentzian method (GL30). The difference between the Ni 2p 1/2 and 3/2 peaks was set to be 17.5 eV. Binding energies at around 852.7 eV and 870.2 eV could be assigned to NiS, while the peaks at 855.2 eV and 872.7 eV indicated the higher valence state of Ni species other than Ni^{2+}. **c**, The corresponding magnified TEM image showing NiS_x nanoparticles (indicated by white arrows). **d**, High-resolution TEM image of a single NiS_x nanoparticle. The larger interplanar spacing (0.31 nm) shown in **d** than that of the (100) plane in NiS (0.29 nm), as well as the defective lattice arrangement, implies the formation of NiS_x.

As a further extension, NiS_x was replaced by a more common Pt co-catalyst. Pt nanoparticles with an average size of 15 nm were firstly synthesized by a one-pot wet-chemistry synthesis (Supplementary Fig. 16). They are actually characterized by branched structures. The same photocatalytic reaction by using Pt as a colloidal co-catalyst was then carried out. The resultant composite photocatalyst was denoted as Twin-Pt-I. An optimized Pt content of 1 wt% was obtained according to our concentration-dependent experiments (Supplementary Fig. 17). Figure 5a shows the time-course performance of H_2 evolution from the 1 wt% Pt-containing photocatalytic reaction. The activity could be significantly enhanced by introducing Pt co-catalyst (Fig. 5a, point 1). In addition to the very high quantum efficiency of about 83% at 425 nm, the Twin-Pt-I photocatalyst was also found with similar photocatalytic behaviour to Twin-Ni-I photocatalyst, however, with a little difference. When we separated Pt from CZS nanoparticles by using centrifugation, instead of obtaining the intrinsic activity of CZS, we still observed an enhancement (Fig. 5a, points 2 and 3). The reason for this could be attributed to the large particle size of Pt that could also be separated from the reaction system with low-speed centrifugation as supported by the TEM and ICP-MS investigation on the samples prepared from the reaction suspension at point 2 in Fig. 5a. As shown in Fig. 5b, although a small fraction of the Pt nanoparticles were found on the surface of CZS nanoparticles during drying the copper grid, isolated Pt nanoparticles on the grid suggest that a collision-contact mechanism may also be at play. ICP-MS test indicated that only 27% of the added Pt nanoparticles were left in the reaction solution. By re-addition of such an amount of Pt nanoparticle (27%, Fig. 5a, point 4), the activity of Twin-Pt-I could be again restored. The similar enhancement by using isolated Pt nanoparticles also suggests the positive role of colloid co-catalyst to obtain the high efficiency by collision mechanism.

We then explored whether the catalytic system could be applied in near-neutral reaction solution by using 30 vol% methanol instead of Na_2S-Na_2SO_3 (pH ≈ 7.87). Notably, in this case, NiS_x was firstly prepared by injecting 1 wt% Ni^{2+} into a Na_2S-Na_2SO_3 solution and separated by an ultracentrifugation method (50,000 r.p.m., 30 min). The obtained NiS_x was then re-dispersed into the methanol solution. Interestingly, a relatively high activity for H_2 evolution over this reaction suspension can still be obtained, with quantum efficiency of about 65% at 425 nm. It implies that the photogenerated holes from CZS nanotwins can be utilized for methanol oxidation without requiring high pH. More importantly, the fact that the colloidal NiS_x in methanol showed similar catalytic behaviour as in

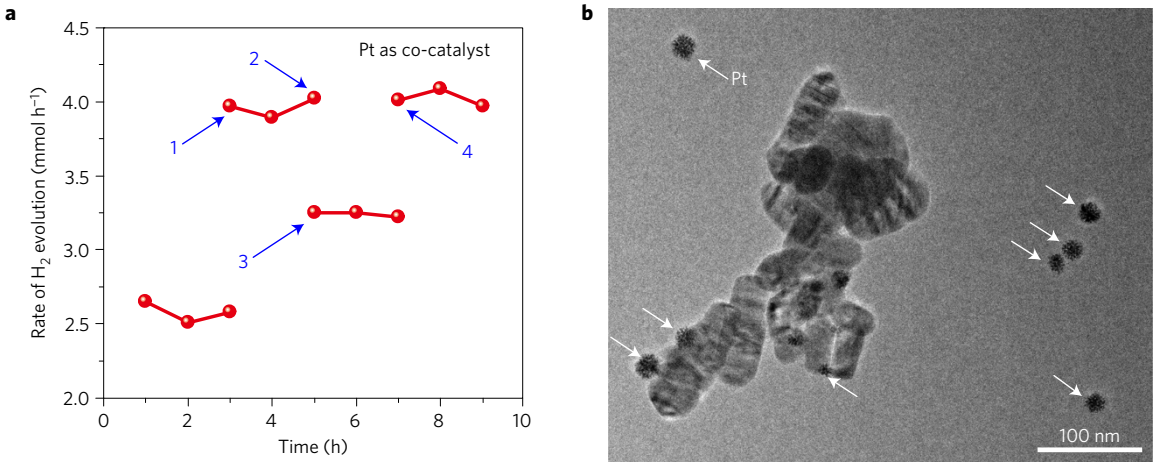

Figure 5 | Photocatalytic performance and characterization of the Twin-Pt-I photocatalyst. a, Photocatalytic activity of the Twin-Pt-I photocatalyst. The reaction was initiated by use of naked CZS powder photocatalyst. After 3-h reaction, 1 wt% Pt nanoparticles were added into the reaction (point 1). After a further 3 h, the reaction suspension was centrifuged (4,000 r.p.m., 10 min, point 2). It was then re-dispersed into a fresh reaction solution (point 3) to conduct the same photocatalytic reaction. The activity was recovered by adding additional Pt nanoparticles into the reaction to maintain the original concentration of Pt (1 wt%, point 4). Note that all reaction conditions were kept the same as that used in Fig. 1c except for the use of a certain amount of Pt instead of NiS_x. **b**, TEM image of the Twin-Pt-I photocatalyst obtained at point 2. Since the Pt nanoparticles have a relatively large particle size (~15 nm), some of them as indicated by white arrows could be still separated from the suspension even under the very low rate of centrifugation.

the S^{2-}/SO_3^{2-} solution (Supplementary Fig. 18) indicates that our proposed collision-contact mechanism may be extended to other photocatalytic system as well.

Conclusions

In summary, the rate of H_2 evolution over CZS twinned photocatalyst can be enhanced by coupling it with a freestanding subnanometre NiS_x co-catalyst. The internal quantum efficiency for water reduction, using Na_2S/Na_2SO_3 as hole scavengers, approaches 100% without introducing any noble metals. Different from a traditional heterojunction that depends on close interconnection between photocatalyst and co-catalyst, a collision-contact mechanism is proposed. Frequent collisions between CZS nanorods and NiS_x clusters are suggested to facilitate the transfer of photogenerated electrons to the clusters and back reaction can be impeded, leading to high utilization efficiency of photogenerated charges in the suspension. Data consistent with a similar mechanism were also obtained for other photocatalytic systems, with different light absorbers and co-catalysts. This work not only presents the possibility for the use of Twin-Ni-I as a potential valuable component for photoinduced hydrogen production, but also advances our knowledge on photocatalyst–co-catalyst interactions to enhance photocatalytic activity.

Methods

Synthesis of $Cd_{0.5}Zn_{0.5}S$ (CZS) photocatalysts. CZS powder photocatalyst with a twin structure in the form of a nanorod was synthesized according to our previous reported methods[28]. Specifically, it was prepared by sequentially adding 10 ml of ethanediamine (EN) and 25 mmol thioacetamide (TAA) to a 40-ml aqueous solution containing 10 mmol $Cd(CH_3COO)_2$ and 10 mmol $Zn(CH_3COO)_2$. The total volume of the reaction was adjusted to 60 ml by introducing additional water. The entire process was carried out under magnetic stirring. The reaction mixture was further stirred for 20 min, sealed in a 100-ml-capacity Teflon-lined autoclave, and heated to 230 °C at a ramping speed of 30 °C min^{-1} in the presence of microwave irradiation. The reaction was allowed to proceed for 30 min. After cooling, the product was separated by centrifugation (4,000 r.p.m., 10 min), washed several times with deionized water and ethanol, and dried at 80 °C for 5 h in a vacuum oven. CZS film was synthesized by an electrophoretic-deposition process. Typically, two pieces of FTO glass were immersed in the colloidal solution with a separation distance of 1 cm and a d.c. voltage of 40 V was applied for 4 min by a Keithley 2400 sourcemeter. The glass electrodes were then rinsed with ethanol, dried with compressed air, and ready for photocatalytic experiments.

Preparation of various NiS_x-containing CZS photocatalysts. Usually, NiS_x was introduced by *in situ* injecting a certain amount $Ni(CH_3COO)_2$ into the photocatalytic reaction suspension containing Na_2S, Na_2SO_3, and CZS photocatalyst. Note Ni^{2+} was determined in mass concentration with respect to the amount of CZS. The coupled photocatalysts were designated to be Twin-Ni-I since the co-catalyst was in an isolated state. If $Ni(CH_3COO)_2$ was introduced to the Na_2S/Na_2SO_3 solution prior to the addition of CZS photocatalyst, the obtained photocatalysts could be designated to be Twin-Ni-I'. During the reaction, aliquots of the reaction suspension containing NiS_x, Twin-Ni-I, or Twin-Ni-I' catalyst were taken out by a pipette to conduct further characterizations. For the synthesis of CZS and NiS_x with a close-contacted interface, 0.005 M $Ni(CH_3COO)_2$ (0.1 ml) and 0.01 M Na_2S solutions (0.1 ml) were, in sequence, injected into a 20-ml aqueous suspension containing 0.1 g of CZS nanotwins. The mixture was then heated at 60 °C under magnetic stirring. The final powder, designated as Twin-Ni-C (C herein indicates that the two materials were contacted with each other), was obtained after evaporation and dried in a vacuum oven at 80 °C for another 5 h.

Preparation of CdS and NiS_x-containing CdS photocatalysts. NaOH aqueous solution (4 M, 10 ml) was spilt into an aqueous solution (50 ml) containing $Cd(CH_3COO)_2$ (20 mmol). Thioacetamide (TAA 0.025 mol) was then added to the previous solution containing $Cd(OH)_2$ precipitation. The whole process was carried out under magnetic stirring. The mixture was further stirred for 10 min and then sealed in a 100 ml Teflon-lined stainless steel autoclave. After heating at 180 °C for 24 h, the autoclave was allowed to cool to room temperature. Yellow precipitates were collected by centrifugation (4,000 r.p.m., 10 min), washed with deionized water and ethanol several times, and dried at 80 °C for 10 h in a vacuum oven. For synthesis of isolated NiS_x-containing CdS (designated to be CdS-Ni-I), the process was the same as that for Twin-Ni-I except that 0.1 g of CdS was used instead of CZS nanotwins.

Preparation of CdSe and NiS_x-containing CdSe photocatalysts. The Se source was from Na_2SeSO_3, which was prepared by dissolving 0.02 mol of selenium powder into an aqueous solution (100 ml) of Na_2SO_3 (0.5 mol l^{-1}). Then the solution was maintained at 70 °C and refluxed for 5 h with a flow of nitrogen as the protection atmosphere. This Na_2SeSO_3 aqueous solution was stored at 60 °C in a conical beaker for further utilization. Nitrilotriacetic acid (2.28 g) was added into a 20-ml aqueous solution containing 2.02 g of KOH under magnetic stirring to form a transparent solution. Then 2.468 g of $Cd(NO_3)_2 \cdot 4H_2O$ and 40 ml Na_2SeSO_3 solution were sequentially added into the solution with magnetic stirring for another 15 min. The resulting solution was sealed in a 100 ml Teflon-lined stainless steel autoclave, and was heated to 100 °C for 16 h. After cooling, the product was separated by centrifugation (4,000 r.p.m., 10 min), washed with deionized water and ethanol several times and dried at 80 °C for 5 h in a vacuum oven. For synthesis of isolated NiS_x-containing CdSe (designated to be CdSe-Ni-I), the process was the same as that for Twin-Ni-I except that 0.1 g of CdSe was used instead of CZS nanotwins.

Preparation of Pt co-catalyst. In a typical synthesis of Pt nanoparticles, 105 mg of polyvinyl pyrrolidone (PVP) and 60 mg of ascorbic acid (AA) were dissolved in 8 ml of deionized water within a 20-ml vial and heated at 90 °C for 10 min in an oil bath under magnetic stirring. Subsequently, 3 ml K_2PtCl_4 (0.067 M) aqueous solution was rapidly injected into the above reaction solution. The vial was then capped and maintained at 90 °C for 3 h. The product was collected by centrifugation (10,000 r.p.m., 10 min) and washed with deionized water several times to remove excess PVP and other residues. Then the as-obtained sample was dispersed into 5 ml deionized water for further use. Isolated Pt-containing CZS nanotwin is designated as Twin-Pt-I.

Photocatalytic reactions. Photocatalytic reactions of hydrogen production by water splitting were conducted in a gas-closed system with a side irradiation Pyrex cell. Photocatalyst powder (0.1 g) was dispersed by a magnetic stirrer in solution (180 ml) containing sodium sulfide (Na_2S, 0.35 M) and sodium sulfite (Na_2SO_3, 0.25 M) as electron donors. After being evacuated by N_2 gas for over 10 min, the photocatalysts were irradiated by visible light ($\lambda \geq 430$ nm) through a cutoff filter from a Xe lamp. The intensity and number of photons of the two light sources were measured with a fibre optic spectrometer. The amount of H_2 gas was determined by online thermal conductivity detector gas chromatography (NaX zeolite column, thermal conductivity detector, and N_2 carrier) or drainage. For photocatalytic reaction over CZS films, all reaction conditions were kept the same except that the CZS film photocatalyst was employed instead of the powder photocatalyst. Apparent quantum efficiencies (AQEs) were measured using different band-pass filters and an irradiation meter and were defined by the equation (1):

$$\mathrm{AQE} = 2N_{\mathrm{H}}/N_{\mathrm{P}} \quad (1)$$

where N_{H} is the number of evolved H_2 molecules and N_{P} is the number of incident photons. Internal quantum efficiencies (IQEs) were calculated by excluding the absorption of the reactor according to equation (2):

$$\mathrm{IQE} = \mathrm{AQE}/T \quad (2)$$

where T is the light transmittance of the reactor.

Characterizations. The crystallite morphologic micrograph was determined on an FEI Tecnai G2 F30 S-Twin transmission electron microscope at 300 kV and a JEOL ARM200 microscope with a STEM Cs corrector. Diffuse reflectance ultraviolet–visible spectra of the powder sample, band-pass filter, and Pyrex cell were obtained on a Hitachi U-4100 spectrometer equipped with a laboratory sphere diffuse reflectance accessory. X-ray photoelectron spectroscopy data were obtained on a Kratos Axis-Ultra DLD instrument with a monochromatized Al $K\alpha$ line source (150 W). Electron spin properties were measured over a Bruker A300 electron paramagnetic resonance facility that contains a 6" double yoke magnet with a magnetic field strength up to 6.5 kG. The concentrations of Ni ions were determined using a Perkin Elmer inductively coupled plasma mass spectrometer (ICP-MS, NexION 300Q). The particle size and zeta potential were measured by Malvern Zetasizer Nano ZS90 with a testing limit ranging from 0.3 nm to 5μm. Ultracentrifugation was realized on a Thermo Scientific Sorvall WX 100 Ultracentrifuge with a maximum speed of 100,000 r.p.m. and a g force of up to 802,000g.

Received 16 April 2016; accepted 23 August 2016; published 26 September 2016

References

1. Fujishima, A. & Honda, K. Electrochemical photolysis of water at a semiconductor electrode. *Nature* **238**, 37–38 (1972).
2. Chen, X., Shen, S., Guo, L. & Mao, S. S. Semiconductor-based photocatalytic hydrogen generation. *Chem. Rev.* **110**, 6503–6570 (2010).
3. Walter, M. *et al.* Solar water splitting cells. *Chem. Rev.* **110**, 6446–6473 (2010).
4. Kudo, A. & Miseki, Y. Heterogeneous photocatalyst materials for water splitting. *Chem. Soc. Rev.* **38**, 253–278 (2009).
5. Hisatomi, T., Kubota, J. & Domen, K. Recent advances in semiconductors for photocatalytic and photoelectrochemical water splitting. *Chem. Soc. Rev.* **43**, 7520–7535 (2014).
6. Zhang, W., Wang, Y., Wang, Z., Zhong, Z. & Xu, R. Highly efficient and noble metal-free NiS/CdS photocatalysts for H_2 evolution from lactic acid sacrificial solution under visible light. *Chem. Commun.* **46**, 7631–7633 (2010).
7. Zhang, K. & Guo, L. Metal sulphide semiconductors for photocatalytic hydrogen production. *Catal. Sci. Technol.* **3**, 1672–1690 (2013).
8. Wang, D., Zou, Z. & Ye, J. Photocatalytic water splitting with the Cr-doped $Ba_2In_2O_5/In_2O_3$ composite oxide semiconductors. *Chem. Mater.* **17**, 3255–3261 (2005).
9. Li, Y. H. *et al.* Unidirectional suppression of hydrogen oxidation on oxidized platinum clusters. *Nat. Commun.* **4**, 2500 (2013).
10. Ma, S. S. K., Hisatomi, T., Maeda, K., Moriya, Y. & Domen, K. Enhanced water oxidation on Ta_3N_5 photocatalysts by modification with alkaline metal salts. *J. Am. Chem. Soc.* **134**, 19993–19996 (2012).
11. Tada, H., Mitsui, T., Kiyonaga, T., Akita, T. & Tanaka, K. All-solid-state Z-scheme in CdS-Au-TiO_2 three-component nanojunction system. *Nat. Mater.* **5**, 782-786 (2006).
12. Wang, H. *et al.* Semiconductor heterojunction photocatalysts: design, construction, and photocatalytic performances. *Chem. Soc. Rev.* **43**, 5234–5244 (2014).
13. Xiang, Q., Yu, J. & Jaroniec, M. Synergetic effect of MoS_2 and graphene as cocatalysts for enhanced photocatalytic H_2 production activity of TiO_2 nanoparticles. *J. Am. Chem. Soc.* **134**, 6575–6578 (2012).
14. Li, Y. H., Peng, C., Yang, S., Wang, H. F. & Yang, H. G. Critical roles of co-catalysts for molecular hydrogen formation in photocatalysis. *J. Catalys.* **330**, 120–128 (2015).
15. Li, H., Zhou, Y., Tu, W., Ye, J. & Zou, Z. State-of-the-art progress in diverse heterostructured photocatalysts toward promoting photocatalytic performance. *Adv. Funct. Mater.* **25**, 998–1013 (2015).
16. Kalisman, P., Nakibli, Y. & Amirav, L. Perfect photon-to-hydrogen conversion efficiency. *Nano Lett.* **16**, 1776–1781 (2016).
17. Maeda, K. & Domen, K. Photocatalytic water splitting: recent progress and future challenges. *J. Phys. Chem. Lett.* **1**, 2655–2661 (2010).
18. Ran, J., Zhang, J., Yu, J., Jaroniec, M. & Qiao, S. Z. Earth-abundant cocatalysts for semiconductor-based photocatalytic water splitting. *Chem. Soc. Rev.* **43**, 7787–7812 (2014).
19. Yang, J., Wang, D., Han, H. & Li, C. Roles of cocatalysts in photocatalysis and photoelectrocatalysis. *Acc. Chem. Res.* **46**, 1900–1909 (2013).
20. Han, Z., Qiu, F., Eisenberg, R., Holland, P. L. & Krauss, T. D. Robust photogeneration of H_2 in water using semiconductor nanocrystals and a nickel catalyst. *Science* **338**, 1321-1324 (2012).
21. Miseki, Y., Kato, H. & Kudo, A. Water splitting into H_2 and O_2 over niobate and titanate photocatalysts with (111) plane-type layered perovskite structure. *Energy Environ. Sci.* **2**, 306–314 (2009).
22. Choi, J., Ryu, S. Y., Balcerski, W., Lee, T. K. & Hoffmann, M. R. Photocatalytic production of hydrogen on Ni/NiO/$KNbO_3$/CdS nanocomposites using visible light. *J. Mater. Chem.* **18**, 2371–2378 (2008).
23. Kato, H., Asakura, K. & Kudo, A. Highly efficient water splitting into H_2 and O_2 over lanthanum-doped $NaTaO_3$ photocatalysts with high crystallinity and surface nanostructure. *J. Am. Chem. Soc.* **125**, 3082–3089 (2003).
24. Tabata, M. *et al.* Photocatalytic hydrogen evolution from water using copper gallium sulfide under visible-light irradiation. *J. Phys.Chem. C* **114**, 11215–11220 (2010).
25. Yan, Z., Wu, H., Han, A., Yu, X. & Du, P. Noble metal-free cobalt oxide (CoO_x) nanoparticles loaded on titanium dioxide/cadmium sulfide composite for enhanced photocatalytic hydrogen production from water. *Int. J. Hydrog. Energy* **39**, 13353–13360 (2014).
26. Foo, W. J., Zhang, C. & Ho, G. W. Non-noble metal Cu-loaded TiO_2 for enhanced photocatalytic H_2 production. *Nanoscale* **5**, 759–764 (2013).
27. Zhang, J., Xu, Q., Qiao, S. Z. & Yu, J. Enhanced visible-light hydrogen-production activity of copper-modified $Zn_xCd_{1-x}S$. *ChemSusChem* **6**, 2009–2015 (2013).
28. Liu, M., Jing, D., Zhou, Z. & Guo, L. Twin-induced one-dimensional homojunctions yield high quantum efficiency for solar hydrogen generation. *Nat. Commun.* **4**, 2278 (2013).
29. Liu, M., Wang, L., Lu, G. M., Yao, X. & Guo, L. Twins in $Cd_{1-x}Zn_xS$ solid solution: highly efficient photocatalyst for hydrogen generation from water. *Energy Environ. Sci.* **4**, 1372–1378 (2011).
30. Tsuji, I., Kato, H. & Kudo, A. Visible-light-induced H_2 evolution from an aqueous solution containing sulfide and sulfite over a ZnS–$CuInS_2$–$AgInS_2$ solid-solution photocatalyst. *Angew. Chem.* **117**, 3631–3634 (2005).
31. Kaga, H. & Kudo, A. Cosubstituting effects of copper(I) and gallium(III) for $ZnGa_2S_4$ with defect chalcopyrite structure on photocatalytic activity for hydrogen evolution. *J. Catalys.* **310**, 31–36 (2014).
32. Simon, T. *et al.* Redox shuttle mechanism enhances photocatalytic H_2 generation on Ni-decorated CdS nanorods. *Nat. Mater.* **13**, 1013–1018 (2014).
33. Moulder, J. F., Chastain, J. & King, R. C. *Handbook of X-ray Photoelectron Spectroscopy: a Reference Book of Standard Spectra for Identification and Interpretation of XPS Data* (Perkin-Elmer Eden Prairie, 1992).
34. Trasatti, S. Electronegativity, work function, and heat of adsorption of hydrogen on metals. *J. Chem. Soc. Faraday Trans. 1* **68**, 229–236 (1972).
35. Trasatti, S. Work function, electronegativity, and electrochemical behaviour of metals: III. Electrolytic hydrogen evolution in acid solutions. *J. Electroanal. Chem.* **39**, 163–184 (1972).
36. Vilekar, S. A., Fishtik, I. & Datta, R. Kinetics of the hydrogen electrode reaction. *J. Electrochem. Soc.* **157**, B1040–B1050 (2010).

37. Skúlason, E. *et al.* Modeling the electrochemical hydrogen oxidation and evolution reactions on the basis of density functional theory calculations. *J. Phys. Chem. C* **114**, 18182–18197 (2010).
38. Jing, D., Hu, Y., Liu, M., Wei, J. & Guo, L. Preparation of highly dispersed nanofluid and CFD study of its utilization in a concentrating PV/T system. *Solar Energy* **112**, 30–40 (2015).
39. Yan, H. *et al.* Visible-light-driven hydrogen production with extremely high quantum efficiency on Pt-PdS/CdS photocatalyst. *J. Catalys.* **266**, 165–168 (2009).

Acknowledgements

This work was supported by the National Nature Science Foundation of China (No. 51236007, No. 51502240), the Natural Science Foundation of Jiangsu Province (No. BK20150378), China Postdoctoral Science Foundation (No. 2014M560769), and the China Fundamental Research Funds for the Central Universities. We also appreciate the help of J. N. Wang, F. Xue, W. Long and P. H. Guo for assistance and thank D. W. Jing for helpful discussions and critical reading of the manuscript.

Author contributions

L.G., M.L. and Y.C. conceived and designed the experiments. L.G. supervised the project. M.L. and Y.C. prepared the powder and film catalysts and analysed the data. M.L., J.Z.S., J.W.S. and X.W. performed the characterizations including XRD, ultraviolet–visible, TEM and so on. M.L. and L.G. prepared and revised the manuscript. All authors discussed the results and commented on the manuscript.

Additional information

Supplementary information is available for this paper. Reprints and permissions information is available at www.nature.com/reprints. Correspondence and requests for materials should be addressed to M.L. or L.G.

Competing interests

The authors declare no competing financial interests.